

Crosstalk Analysis of *E*-Plane Ku Band Waveguide Joints

Neelam Sharma* and Debendra K. Panda

Abstract—This paper presents crosstalk analysis of *E*-plane multichannel waveguide joints for high frequency. The multi-cavity modeling technique and method of moment are used to analyze the crosstalk. Waveguide has many practical uses in high powered RF systems. When two channel waveguides are joined, the phenomenon of crosstalk will certainly appear, and the reason behind is poor workmanship. The gap appearing at the flange joint causes power coupling to the neighboring ports. In this paper, two channel *E*-plane waveguide joints for frequency range 15 GHz to 18 GHz have been analyzed. Scattering parameters data obtained from cavity model analysis have been verified and compared with CST microwave studio simulated and measured data.

1. INTRODUCTION

Waveguides are used as a transmission line in microwave communications, broadcasting, and RADAR installation. Two-dimensional phased array antennas have wide applications in communication satellite, RADAR detection of missile, Wi-Fi, and multiple-input multiple-output (MIMO). At the input of phased array antenna multiport power dividers or combiners are mainly used. Whenever 2 channel waveguides are joined, due to faulty workmanship at the joint, field may couple to the neighboring channel, and crosstalk will appear. Crosstalk is an issue for many applications such as RADAR communication, satellite communication, and mobile communication. Many authors have described crosstalk in coaxial cables, microstrip lines, and optical fiber cables [1–4]. Although the problem of coupling in waveguide has been analyzed for X-band [10, 11], no work has been done on crosstalk analysis for high frequency bands. Frequency scaling cannot be applied to the prototype design due to standard waveguide specification such as wall thickness. For high frequency band applications, there is necessity of new investigations.

In the present scenario, the demand of higher frequency bands is increasing to meet the requirement of 5G technology. Due to faulty workmanship, there is possibility of crosstalk. So, at higher frequency bands crosstalk should be analyzed. Various researches are going on longitudinal waveguide for high power transmission and radiation. There is necessity to use waveguide component for high frequency applications. Hence, this problem is discussed.

Multi-Cavity Modeling is an excellent technique for the analysis of waveguide-based components. It was proposed by Vengadarajan [5]. After that Das, Chakraborty, and Panda used cavity model technique for analysis of power dividers and combiners [6–8]. Cavity modeling is even used for the analysis of waveguide-based network for high frequency [12]. This paper presents the analysis of coupling at waveguide joints using method of moment and multi-cavity modeling. This technique involves replacing all the aperture and discontinuities of the waveguide structures with an equivalent magnetic current density so that the given structure can be analyzed using Magnetic Field Integral Equation (MFIE). To model the crosstalk, a uniform gap is added at waveguide joints. The gap is surrounded by conductor walls to form a cavity. Further the tangential component of magnetic field scattered inside the waveguide and cavities are determined using the procedure outlined in [8], and the

Received 16 July 2021, Accepted 6 September 2021, Scheduled 17 September 2021

* Corresponding author: Neelam Sharma (neelam2407sharma@gmail.com).

The authors are with the Department of Electronics Engineering, Medicaps University, Indore, M.P. 453331, India.

continuity of tangential component of magnetic field at coupling aperture is also considered. Now to solve for the electric field at the window aperture, method of moment is used. In this method, basis functions are used to convert all the integral equations into matrix equations. By the knowledge of aperture fields, reflection and transmission coefficients are evaluated. Since the length and width of coupling region (or cavity) are of arbitrary dimension, the cross-polarization component has also been considered in analysis. This technique can also be used for other higher bands.

2. ANALYSIS OF WAVEGUIDE CROSSTALK

For the analysis of cross talk, two channels are formed using two waveguides connected with each other with a finite gap as shown in Fig. 1, and its cavity modeling and details of region are shown in Fig. 2. It may be noted that the structure has five regions namely waveguide 1, cavity gap, waveguide 2, waveguide 3, and waveguide 4 and four interfacing apertures (A_1 – A_4).

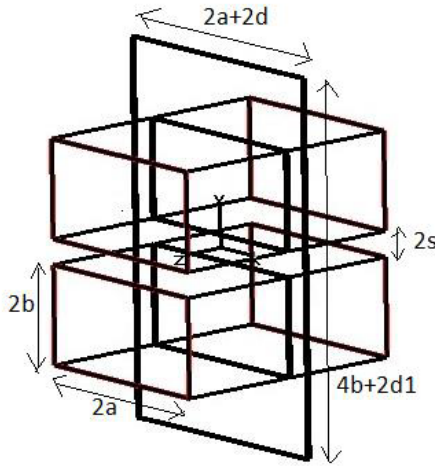


Figure 1. The three-dimensional view of two channel E -plane waveguides with gap.

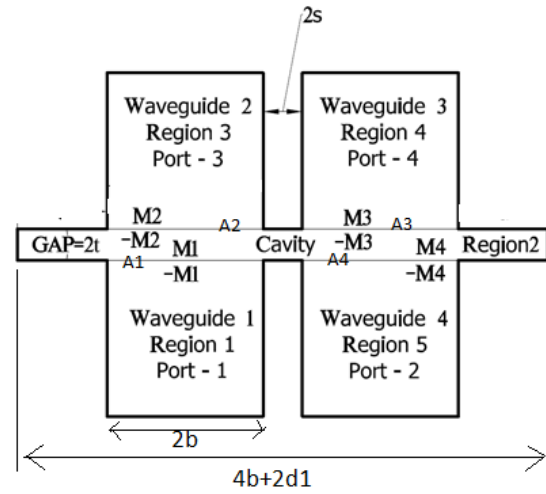


Figure 2. Cavity modeling and details of regions of an E -plane two channel waveguide joints.

The interfacing apertures between different regions are replaced by equivalent magnetic current densities [9]. As there are four apertures, there are four magnetic current densities M_1 , M_2 , M_3 , and M_4 . These are considered as source and can be determined by cavity Green's function for cavity region and modal expansion method for waveguide regions (W_1 – W_4) [10]. Boundary conditions can be found between different regions by applying the continuity of tangential component of magnetic field across the apertures as given by:

Aperture-1, Region 1 = Region 2

$$H_y^{wvg.1}(M_1^y) + H_y^c(M_1^y) + H_y^{wvg.1}(M_1^z) + H_y^c(M_1^z) - H_y^c(M_2^y) - H_y^c(M_2^z) - H_y^c(M_3^y) - H_y^c(M_3^z) + H_y^c(M_4^y) + H_y^c(M_4^z) = 2H_y^{in} \quad (1)$$

$$H_z^{wvg.1}(M_1^y) + H_z^c(M_1^y) + H_z^{wvg.1}(M_1^z) + H_z^c(M_1^z) - H_z^c(M_2^y) - H_z^c(M_2^z) - H_z^c(M_3^y) - H_z^c(M_3^z) + H_z^c(M_4^y) + H_z^c(M_4^z) = 0 \quad (2)$$

Aperture-2, Region 2 = Region 3

$$H_y^{wvg.2}(M_2^y) - H_y^c(M_1^y) + H_y^{wvg.2}(M_2^z) - H_y^c(M_1^z) + H_y^c(M_2^y) + H_y^c(M_2^z) + H_y^c(M_3^y) + H_y^c(M_3^z) - H_y^c(M_4^y) - H_y^c(M_4^z) = 0 \quad (3)$$

$$H_z^{wvg.2}(M_2^y) - H_z^c(M_1^y) + H_z^{wvg.2}(M_2^z) - H_z^c(M_1^z) + H_z^c(M_2^y) + H_z^c(M_2^z) + H_z^c(M_3^y) + H_z^c(M_3^z) - H_z^c(M_4^y) - H_z^c(M_4^z) = 0 \quad (4)$$

Aperture-3, Region 2 = Region 4

$$H_y^{wvg-3}(M_3^y) - H_y^c(M_1^y) + H_y^{wvg-3}(M_3^z) - H_y^c(M_1^z) + H_y^c(M_2^y) + H_y^c(M_2^z) + H_y^c(M_3^y) + H_y^c(M_3^z) - H_y^c(M_4^y) - H_y^c(M_4^z) = 0 \quad (5)$$

$$H_z^{wvg-3}(M_3^y) - H_z^c(M_1^y) + H_z^{wvg-3}(M_3^z) - H_z^c(M_1^z) + H_z^c(M_2^y) + H_z^c(M_2^z) + H_z^c(M_3^y) + H_z^c(M_3^z) - H_z^c(M_4^y) - H_z^c(M_4^z) = 0 \quad (6)$$

Aperture-4, Region 2 = Region 5

$$H_y^{wvg-4}(M_4^y) + H_y^c(M_1^y) + H_y^{wvg-4}(M_4^z) + H_y^c(M_1^z) - H_y^c(M_2^y) - H_y^c(M_2^z) - H_y^c(M_3^y) - H_y^c(M_3^z) + H_y^c(M_4^y) + H_y^c(M_4^z) = 0 \quad (7)$$

$$H_z^{wvg-4}(M_4^y) + H_z^c(M_1^y) + H_z^{wvg-4}(M_4^z) + H_z^c(M_1^z) - H_z^c(M_2^y) - H_z^c(M_2^z) - H_z^c(M_3^y) - H_z^c(M_3^z) + H_z^c(M_4^y) + H_z^c(M_4^z) = 0 \quad (8)$$

Electric and magnetic fields are represented over y - z plane. So y component of incident magnetic field at the aperture is a dominant TE₁₀ mode and is given by

$$H_y^{in} = -Y_0 \cos\left(\frac{\pi y}{2a_i}\right) e^{-j\beta x}$$

As field distributions are unknown, but can be expressed as the weighted sum of sinusoidal basis functions, they can be given as

$$\vec{E} = \hat{y} \sum_{p=1}^M E_p^{i,y} e_p^{i,y} + \hat{z} \sum_{p=1}^M E_p^{i,z} e_p^{i,z} \quad (9)$$

Here $E_p^{i,y/z}$ are the unknown weights, and $e_p^{i,y/z}$ are the sinusoidal basis function which is given by:

$$e_p^{i,z} = \begin{cases} \sin\left\{\frac{p\pi}{2L}(y - y_w + L)\right\} & \text{for } y_w - L \leq y \leq y_w + L, \\ & z_w - W \leq z \leq z_w + W \\ 0 & \text{elsewhere} \end{cases} \quad (10a)$$

$$e_p^{i,y} = \begin{cases} \sin\left\{\frac{p\pi}{2W}(z - z_w + W)\right\} & \text{for } y_w - L \leq y \leq y_w + L, \\ & z_w - W \leq z \leq z_w + W \\ 0 & \text{elsewhere} \end{cases} \quad (10b)$$

In the above expressions $L = a$, $W = b$, where $2a = 15.799$ mm, $2b = 7.899$ mm, $s = 1.02$ mm, and $2s$ is the distance between waveguide-1 and waveguide-4.

To determine the aperture field distributions, unknown weight $E_p^{i,y/z}$ must be determined. There are four boundaries (A_1 - A_4) shown in Figure 2, and for each boundary there are two boundary conditions, corresponding to the two tangential components (Y and Z). Since each component of field is described by M basis functions, $8M$ unknowns are to be determined from the boundary conditions. Boundary conditions have been solved using Galerkin's specialization of the method of moment [13]. The weighting functions $w_q^{i,y/z}(x, y, z)$ are assumed to be the same as basis functions $e_p^{i,y/z}$.

3. REFLECTION COEFFICIENT AND TRANSMISSION COEFFICIENT

Reflection and transmission coefficients have been derived as the procedure outlined in [8]. The reflection coefficient Γ can then be expressed as

$$S_{11} = \Gamma = \frac{E_z^1 + E_z^2}{E_z^{inc}} = -1 + \frac{W_i L_i}{a_i b_i} \sum_{p=1}^M E_p^{i,z} \left[\cos\left\{\frac{\pi}{2}\left(-\frac{y_w}{a_i} - p + 1\right)\right\} \operatorname{sinc}\left\{\frac{\pi L}{2}\left(\frac{p}{L} - \frac{1}{a_i}\right)\right\} - \cos\left\{\frac{\pi}{2}\left(-\frac{y_w}{a_i} + p + 1\right)\right\} \operatorname{sinc}\left\{\frac{\pi L}{2}\left(\frac{p}{L} + \frac{1}{a_i}\right)\right\} \right] = -1 - E_1^{1,z} \quad (11)$$

The transmission coefficient is given by

$$S_{21/31/41} = T_{j,i} = \frac{E_z^{\text{transmitted}}}{E_z^{\text{inc}}} = \frac{W_j L_j}{a_j b_j} \sum_{p=1}^M E_p^{i,z} \left[\cos \left\{ \frac{\pi}{2} \left(-\frac{y_w}{a_j} - p + 1 \right) \right\} \operatorname{sinc} \left\{ \frac{\pi L}{2} \left(\frac{p}{L} - \frac{1}{a_j} \right) \right\} - \cos \left\{ \frac{\pi}{2} \left(-\frac{y_w}{a_j} + p + 1 \right) \right\} \operatorname{sinc} \left\{ \frac{\pi L}{2} \left(\frac{p}{L} + \frac{1}{a_j} \right) \right\} \right] = - \left(E_1^{2/3/4,z} \right) \quad (12)$$

4. RESULT AND DISCUSSION

For the measurement purpose, E -plane bends are joined together with a common flange and metallic plate as shown in Figure 3. On the basis of formulation, MATLAB codes have been written to compute the reflection and transmission coefficients. MCMT data for magnitude of S -parameter of an E -plane WR-62 waveguide joints with two channels at Ku-band have been compared with CST microwave Studio

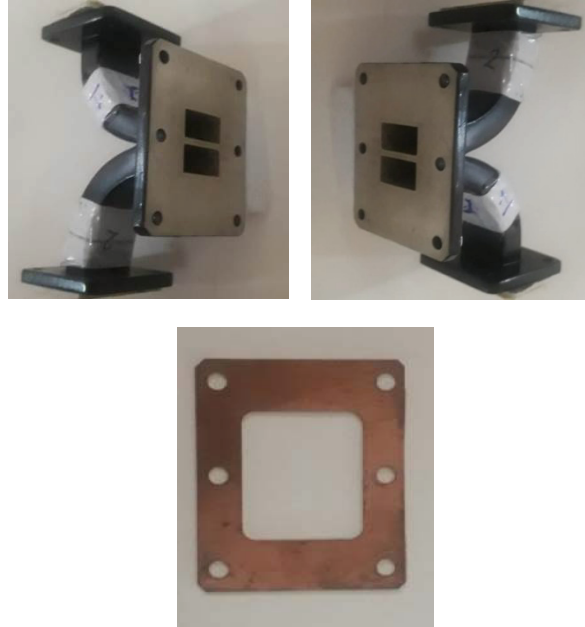


Figure 3. Photograph of two channel E -plane waveguide bends with metallic plate.

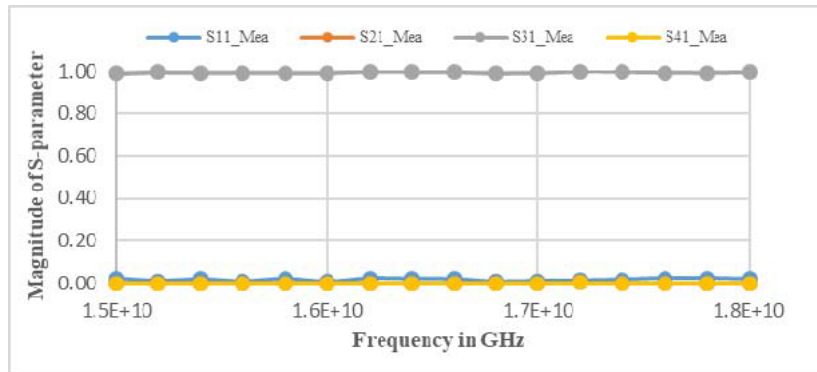
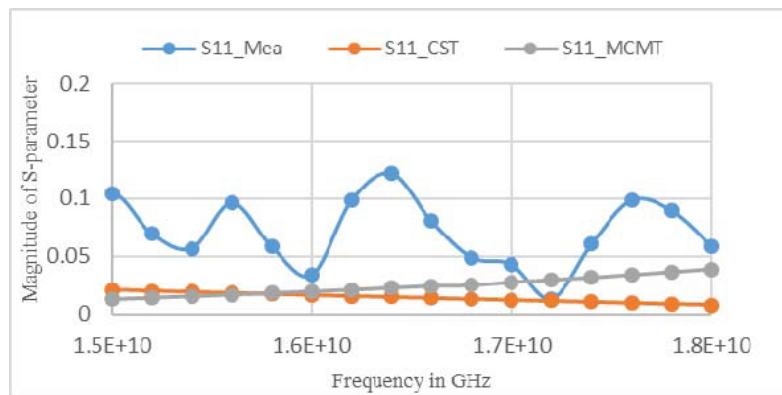


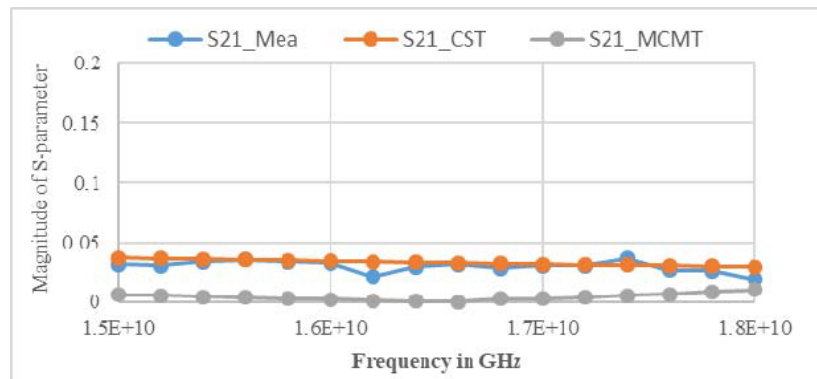
Figure 4. Measured data for an E -plane WR-62 waveguide two channel joints for Ku-band without gap.

simulated data as well as with measured data. The scattering parameters for the circuit, when it is excited through port 2, port 3, and port 4, have not been presented in this paper because they also provide the same pattern of data as for port 1.

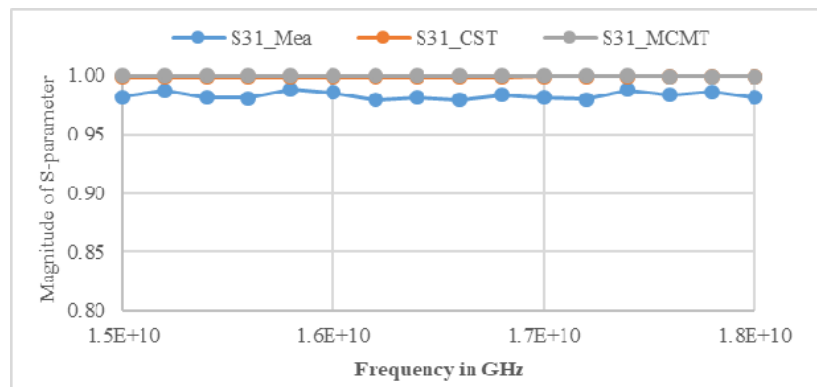
Initially, the measurement of magnitude of S -parameter for frequency range 15 GHz to 18 GHz of E -plane WR-62 waveguide two channel joints without gap has been done by Vector Network Analyzer (Agilent Technologies, E8363B, MY43030518, and A.06.04.32) which is shown in Figure 4. The magnitudes of S -parameters for Ku-band E -plane WR-62 waveguide two channel joints with a gap of $2t = 0.5$ mm, $d = 2.1$ mm and $d1 = 2.1$ mm are shown in Figures 5(a) to 5(d). In Figures 6(a) to 6(d), the magnitudes of S -parameter for frequency range 15 GHz to 18 GHz are shown when port-1 is excited for $2t = 0.3$ mm, $d = 2.1$ mm, and $d1 = 7.1$ mm. The magnitudes of S -parameter for Ku-band E -plane WR-62 waveguide two channel joints with a gap of $2t = 0.5$ mm, $d = 4.6$ mm, and



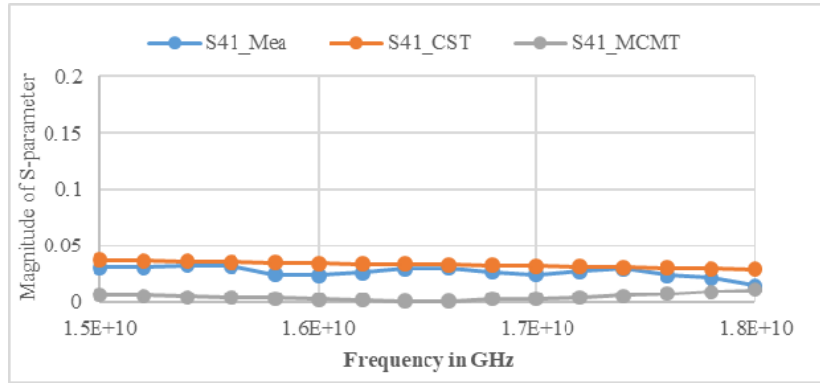
(a)



(b)

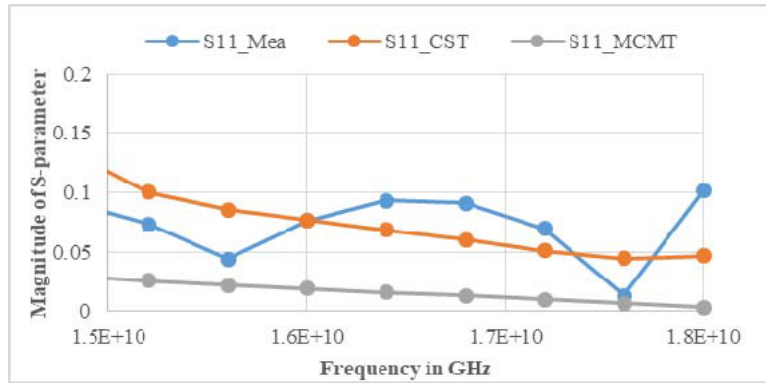


(c)

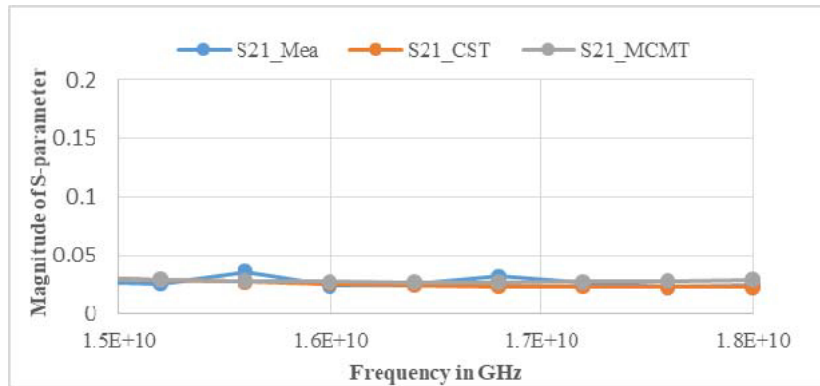


(d)

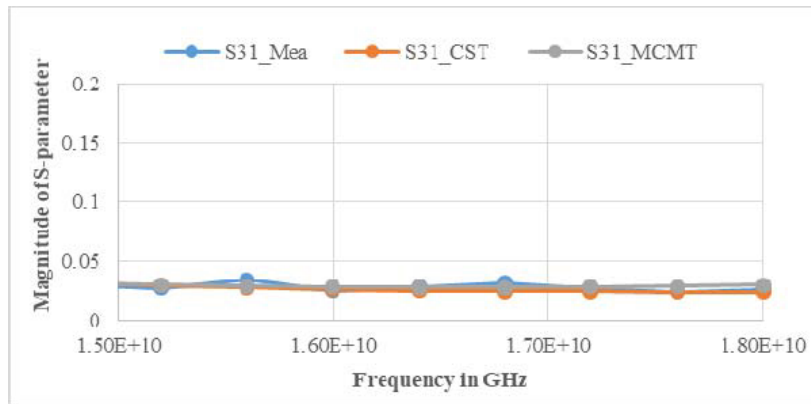
Figure 5. (a) Comparison of S_{11} parameter of MCMT, CST Microwave Studio simulated data and measured data for an E -plane WR-62 waveguide two channel joints for Ku-band with gap of $2t = 0.5$ mm, $d = 2.1$ mm and $d1 = 2.1$ mm. (b) Comparison of S_{21} parameter of MCMT, CST Microwave Studio simulated data and measured data for an E -plane WR-62 waveguide two channel joints for Ku-band with gap of $2t = 0.5$ mm, $d = 2.1$ mm and $d1 = 2.1$ mm. (c) Comparison of S_{31} parameter of MCMT, CST Microwave Studio simulated data and measured data for an E -plane WR-62 waveguide two channel joints for Ku-band with gap of $2t = 0.5$ mm, $d = 2.1$ mm and $d1 = 2.1$ mm. (d) Comparison of S_{41} parameter of MCMT and CST Microwave Studio simulated data and measured data for an E -plane WR-62 waveguide two channel joints for Ku-band with gap of $2t = 0.5$ mm, $d = 2.1$ mm and $d1 = 2.1$ mm.



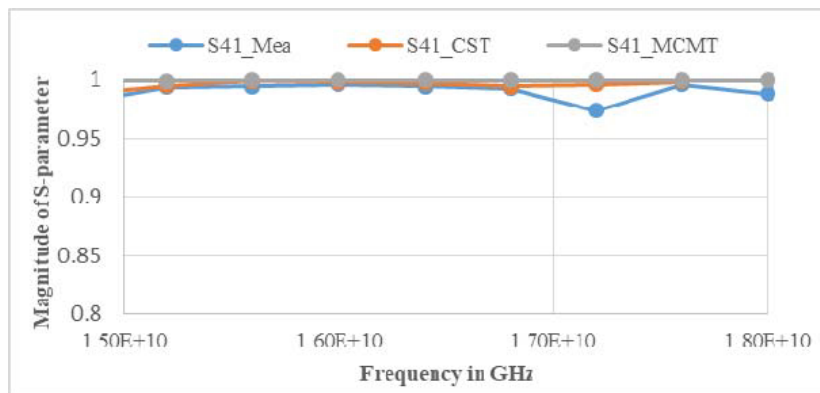
(a)



(b)

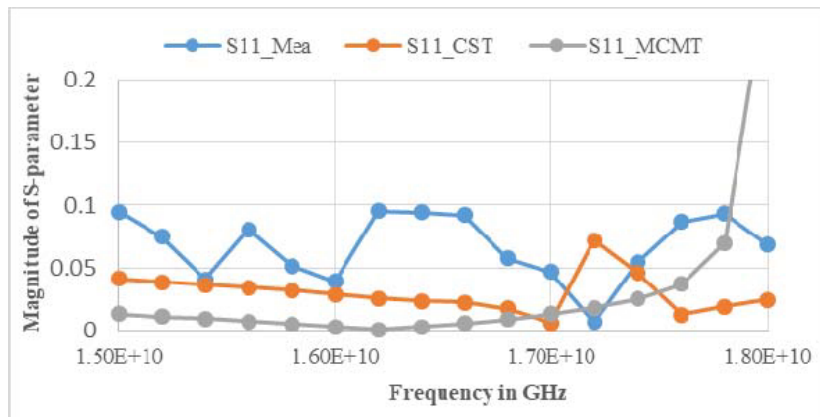


(c)

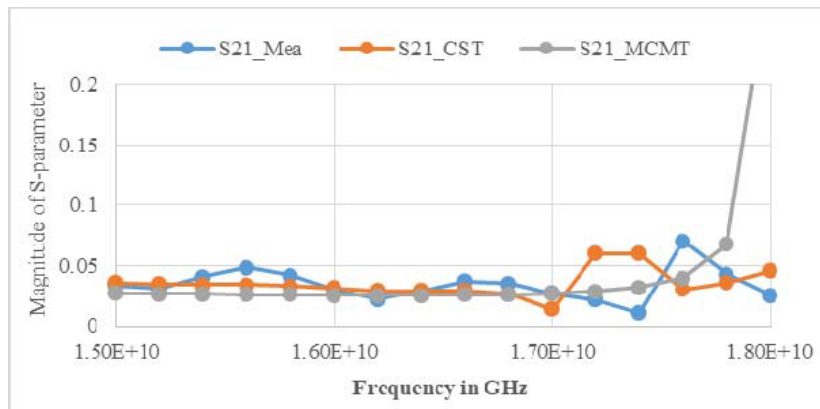


(d)

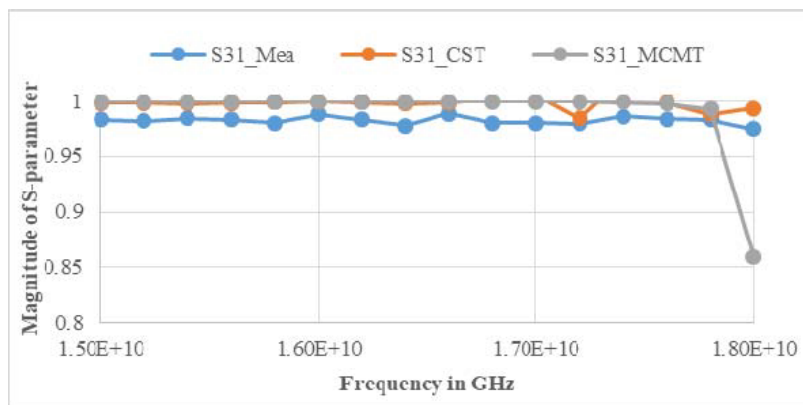
Figure 6. (a) Comparison of S_{11} parameter of MCMT and CST Microwave Studio simulated data and measured data for an E -plane WR-62 waveguide two channel joints for Ku-band with gap of $2t = 0.3$ mm, $d = 2.1$ mm and $d1 = 7.1$ mm. (b) Comparison of S_{21} parameter of MCMT and CST Microwave Studio simulated data and measured data for an E -plane WR-62 waveguide two channel joints for Ku-band with gap of $2t = 0.3$ mm, $d = 2.1$ mm and $d1 = 7.1$ mm. (c) Comparison of S_{31} parameter of MCMT and CST Microwave Studio simulated data and measured data for an E -plane WR-62 waveguide two channel joints for Ku-band with gap of $2t = 0.3$ mm, $d = 2.1$ mm and $d1 = 7.1$ mm. (d) Comparison of S_{41} parameter of MCMT and CST Microwave Studio simulated data and measured data for an E -plane WR-62 waveguide two channel joints for Ku-band with gap of $2t = 0.3$ mm, $d = 2.1$ mm and $d1 = 7.1$ mm.



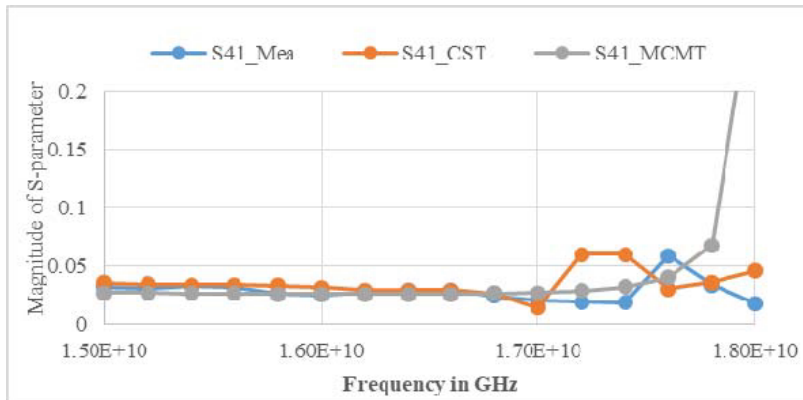
(a)



(b)



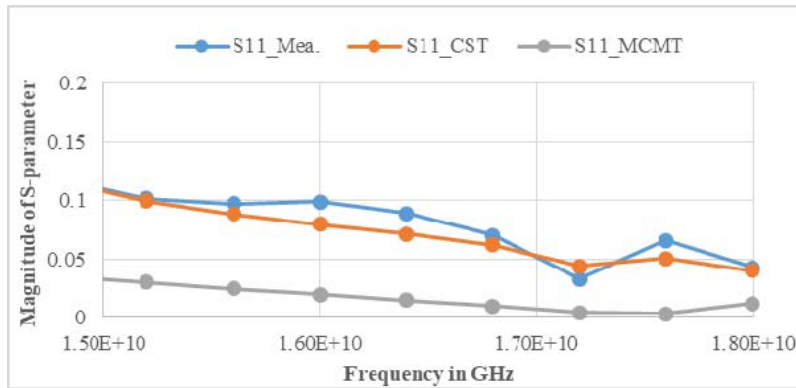
(c)



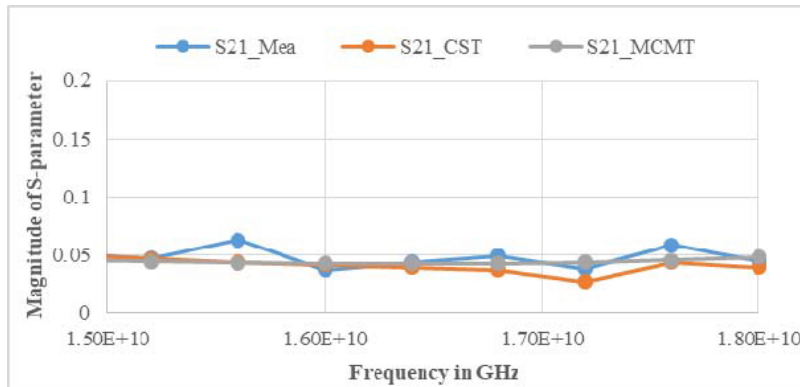
(d)

Figure 7. (a) Comparison of the S_{11} parameter of the MCMT and CST Microwave Studio simulated data and measured data for an E -plane WR-62 waveguide two channel joints for Ku-band with gap of $2t = 0.5$ mm, $d = 4.6$ mm and $d_1 = 9.6$ mm. (b) Comparison of the S_{21} parameter of the MCMT and CST Microwave Studio simulated data and measured data for an E -plane WR-62 waveguide two channel joints for Ku-band with gap of $2t = 0.5$ mm, $d = 4.6$ mm and $d_1 = 9.6$ mm. (c) Comparison of the S_{31} parameter of the MCMT and CST Microwave Studio simulated data and measured data for an E -plane WR-62 waveguide two channel joints for Ku-band with gap of $2t = 0.5$ mm, $d = 4.6$ mm and $d_1 = 9.6$ mm. (d) Comparison of the S_{41} parameter of the MCMT and CST Microwave Studio simulated data and measured data for an E -plane WR-62 waveguide two channel joints for Ku-band with gap of $2t = 0.5$ mm, $d = 4.6$ mm and $d_1 = 9.6$ mm.

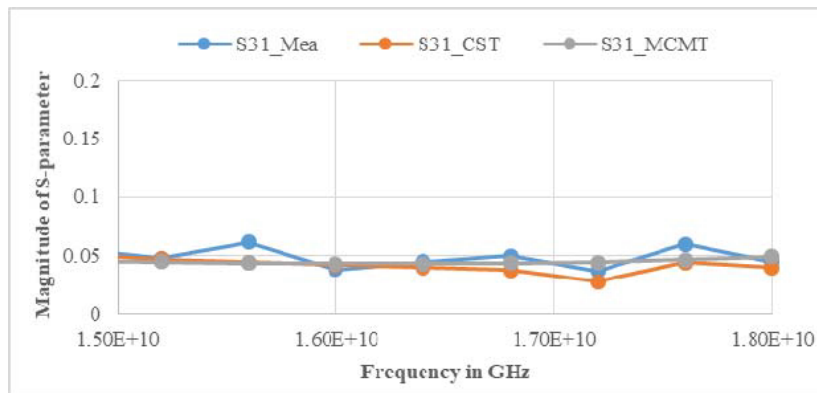
$d1 = 9.6$ mm are shown in Figures 7(a) to 7(d). In Figures 8(a) to 8(d), the magnitudes of S -parameter are shown when port-1 is excited for $2t = 0.5$ mm, $d = 4.6$ mm, and $d1 = 7.1$ mm. It has been analyzed that measured data, MCMT data, and CST simulated data have excellent matching throughout the graph when $2t = 0.5$, $d = 2.1$, and $d1 = 2.1$ and when $2t = 0.3$ mm, $d = 2.1$ mm, and $d1 = 7.1$ mm. Similarly, there is also excellent matching among measured data, MCMT data, and CST simulated data for frequency range 15 GHz to 18 GHz when $2t = 0.5$ mm, $d = 4.6$ mm, and $d1 = 9.6$ mm and when $2t = 0.5$ mm, $d = 4.6$ mm, and $d1 = 7.1$ mm.



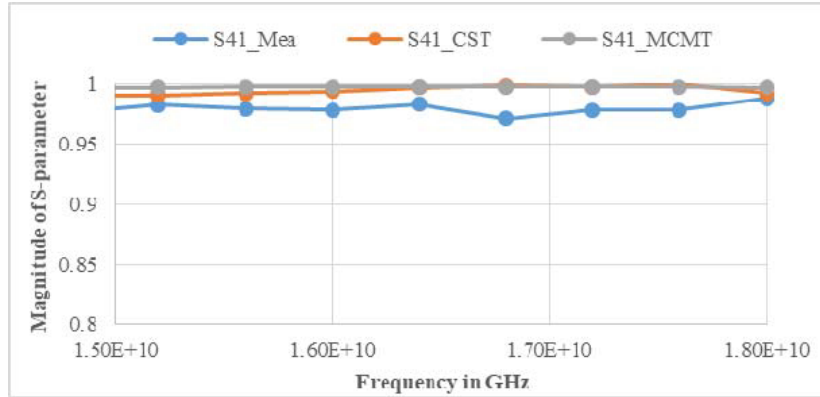
(a)



(b)



(c)



(d)

Figure 8. (a) Comparison of the S_{11} parameter of the MCMT and CST Microwave Studio simulated data and measured data for an E -plane WR-62 waveguide two channel joints for Ku-band with gap of $2t = 0.5$ mm, $d = 4.6$ mm and $d1 = 7.1$ mm. (b) Comparison of the S_{21} parameter of the MCMT and CST Microwave Studio simulated data and measured data for an E -plane WR-62 waveguide two channel joints for Ku-band with gap of $2t = 0.5$ mm, $d = 4.6$ mm and $d1 = 7.1$ mm. (c) Comparison of the S_{31} parameter of the MCMT and CST Microwave Studio simulated data and measured data for an E -plane WR-62 waveguide two channel joints for Ku-band with gap of $2t = 0.5$ mm, $d = 4.6$ mm and $d1 = 7.1$ mm. (d) Comparison of the S_{41} parameter of the MCMT and CST Microwave Studio simulated data and measured data for an E -plane WR-62 waveguide two channel joints for Ku-band with gap of $2t = 0.5$ mm, $d = 4.6$ mm and $d1 = 7.1$ mm.

5. CONCLUSION

In this paper, an attempt has been made to apply Multi-Cavity Modeling Technique to analyze crosstalk in between two channel E -plane waveguide joints for the frequency range 15 GHz to 18 GHz. Scattering parameters for the circuit have been obtained. A generalized algorithm is developed to characterize crosstalk. There is excellent matching of CST simulated data, measured data, and MCMT data. It has been seen that there is no coupling of power to neighboring port of two channel E -plane waveguide joints at Ku-band for the above considered dimensions.

This computation is carried out to analyze crosstalk in a closed metallic region, and as the demand of high frequency band is increasing, there are higher possibilities of crosstalk. This work will be helpful to give insight to the crosstalk between waveguide channels at high frequency and MIMO applications.

ACKNOWLEDGMENT

The support provided by Medicaps University is gratefully acknowledged.

REFERENCES

1. Agapiou, G., T. Doukoglou, P. Georgiadis, G. Georgakopoulos, E. Plakidis, P. Rorris, K. Ioannou, and A. Garpis, "Crosstalk and isolation measurement in copper wires," *International Conference on Information Security, Communication and Computer*, Spain, 2005.
2. Tidjani, N., J. C. Le Bunetel, and A. Ouchar, "An asymmetrical microstrip SPICE model for crosstalk evolution," *International Journal of Circuits, System and Signal Processing*, Vol. 7, No. 6, 329–334, 2013.
3. Balasubramanian, R., Y. Y. Miyazaki, and M. Kondo, "Investigation of crosstalk effects due to optical fiber nonlinearities in WDM CATV network," *Progress In Electromagnetics Research Online*, Vol. 3, No. 6, 940–942, 2007.

4. Roy, A., S. Ghosh, and A. Chakraborty, "Simple cross talk model of three wires to predict near-end and far-end crosstalk in an EMI/EMC modeling," *Progress In Electromagnetics Research B*, Vol. 8, 43–58, 2008.
5. Vengadarajan, A., "Multiple cavity modeling technique for solving aperture coupled waveguide junctions," Ph.D. dissertation, Department of Electronics & Electrical Communication Engineering, Indian Institute of Technology, Kharagpur, 1999.
6. Das, S. and A. Chakraborty, "A novel modeling technique to solve a class of rectangular waveguide based circuit and radiators," *Progress In Electromagnetic Research*, Vol. 61, 231–252, 2006.
7. Das, S., A. Chakraborty, and A. Chakraborty, "Analysis of multiport waveguide power divider/combiner for phased array application," *NCC 2007*, Kanpur, India, 2007.
8. Panda, D. K., "Analysis and design of longitudinal rectangular waveguide power dividers/combiners using multiple cavity modeling technique," Ph. D. Dissertation, Department of Electronics & Electrical Communication Engineering, Indian Institute of Technology, Kharagpur, 2010.
9. Harrington, R. F., *Time Harmonic Electromagnetic Fields*, McGraw-Hill Book Company, New York, 1961.
10. Panda, D. K., A. Chakraborty, and S. Choudhury, "Analysis of co-channel interference at waveguide joints using multiple cavity modeling technique," *Progress In Electromagnetics Research Letters*, Vol. 4, 91–98, 2008.
11. Panda, D. K. and A. Chakraborty, "Cross talk analysis at faulty multi-channel waveguide joints," *International Journal of Microwave and Optical Technology*, Vol. 6, No. 1, 51–56, 2011.
12. Panda, D. K. and A. Chakraborty, "Analysis and design of longitudinal power divider/combiner for higher frequencies," *International Journal of Microwave and Optical Technology*, Vol. 10, No. 4, 240–244, 2015.
13. Harrington, R. F., *Field Computation by Moment Methods*, Roger E. Krieger Publishing Company, USA, 1968.